Inorganic Chemistry

Article

pubs.acs.org/IC

Magnetic and Structural Studies of the Multifunctional Material $SrFe_{0.75}Mo_{0.25}O_{3-\delta}$

M. Retuerto,[†] M.-R. Li,[†] Y. B. Go,[†] A. Ignatov,[‡] M. Croft,[‡] K. V. Ramanujachary,[§] J. Hadermann,[∥] J. P. Hodges,[⊥] R. H. Herber,[#] I. Nowik,[#] and M. Greenblatt*[,†]

[†]Department of Chemistry and Chemical Biology, Rutgers, The State University of New Jersey, 610 Taylor Road, Piscataway, New Jersey, 08854, United States

[‡]Department of Physics and Astronomy, Rutgers, The State University of New Jersey, 136 Frelinghuysen Road, Piscataway, New Jersey, 08854, United States

[§]Department of Chemistry and Physics, Rowan University, 210 Mullica Hill Road, Glassboro, New Jersey, 08028, United States

[∥]EMAT, University of Antwerp, Groenenborgerlaan 171, 2020 Antwerp, Belgium

[⊥]Instrument and Source Design Division, Oak Ridge National Laboratory, Oak Ridge, Tennessee 37831, United States

[#]Racah Institute of Physics, Hebrew University, Jerusalem, 91904 Israel

ABSTRACT: $SrFe_{0.75}Mo_{0.25}O_{3-\delta}$ has been recently discovered as an extremely efficient electrode for intermediate temperature solid oxide fuel cells (IT-SOFCs). We have performed structural and magnetic studies to fully characterize this multifunctional material. We have observed by powder neutron diffraction (PND) and transmission electron microscopy (TEM) that its crystal symmetry is better explained with a tetragonal symmetry (*I*4/*mcm* space group) than with the previously reported orthorhombic symmetry (*Pnma* space group). The temperature dependent magnetic properties indicate an exceptionally high magnetic ordering temperature ($T_N \sim 750$ K), well above room temperature. The ordered magnetic structure at low temperature was determined by PND to be an antiferromagnetic coupling of the Fe cations. Mössbauer spectroscopy corroborated the PND results. A detailed study, with X-ray absorption spectroscopy (XAS), in agreement with the Mössbauer results, confirmed the formal oxidation states of the cations to be mixed valence $Fe^{3+/4+}$ and Mo^{6+}.

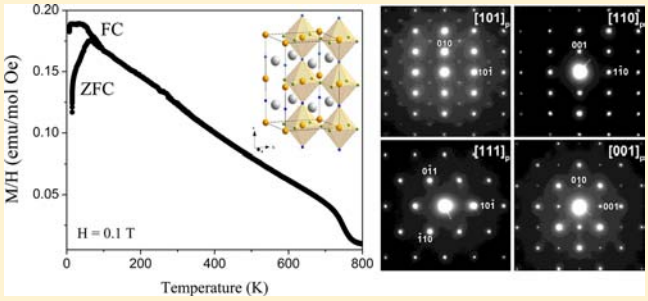

INTRODUCTION

The search for multifunctional materials is a promising area of research due to the interest in fields including multiferroicity, fuel cells, and spintronics. Metal oxides with an ABO_3 perovskite structure have traditionally attracted much attention since they present a variety of promising physical properties for potential applications, such as superconductivity, ferroelectricity, and magnetoresistance. Recently, the perovskites have been investigated also as electrode materials for the development of intermediate-temperature solid oxide fuel cells (IT-SOFCs).[1,2]

Much attention has been focused on the study of perovskites with two types of cations at the B site of the structure. The interest in these so-called double perovskites of general formula $A_2B'B''O_6$ (A = divalent cations or rare earths; B = transition metals) has been renewed due to the room temperature (RT) colossal magnetoresistance (CMR) properties exhibited by Sr_2FeMoO_6.[3] However, only a few metal oxides were found to show the potentially useful properties of this material, which simultaneously exhibits ferromagnetic (FM) and half-metallic behavior at RT. The modification of the compositional, structural, and magnetic properties of Sr_2FeMoO_6 has been widely studied to find candidates for technological devices.[4,5] Similar CMR properties were described for other double perovskites such as A_2FeMoO_6 (A = Ba, Ca)[6,7] and A_2FeReO_6 (A = Sr, Ba, Ca).[8,9]

In this work, we focused on a double perovskite of stoichiometry $Sr_4Fe_3MoO_{12}$ (rewritten as $Sr_2(Fe)_{B'}(Fe_{0.5}Mo_{0.5})_{B''}O_6$) with intrinsic partial disorder between Fe and Mo over half of the perovskite B positions and full occupation of Fe over the other half of B sites. The objective was to improve the magnetic properties of Sr_2FeMoO_6 by increasing the amount of the stronger magnetic cation (Fe^{3+}, d^5) at the B site. This strategy has previously worked for the family of perovskites $A_3Fe_2B''O_9$ (A = Ca, Sr, Ba; B″ = U, Te, Mo).[10−12]

Recently, the interest in $Sr_4Fe_3MoO_{12}$ has been renewed, because of its potential application as efficient electrode material for IT-SOFCs:[13−15] both as a cathode and anode simultaneously, with excellent chemical compatibility with the

Received: July 16, 2012
Published: October 26, 2012

electrolyte and chemical stability in both reducing and oxidizing conditions.[16]

Surprisingly, we found that $Sr_4Fe_3MoO_{12}$, this interesting material for SOFCs, is also an exciting magnetic material, and therefore in this work we carried out detailed magnetic and crystallographic studies to determine its magnetic and crystallographic structure, as well as further characterizations by X-ray absorption spectroscopy (XAS), Mössbauer spectroscopy, and electron diffraction (ED).

EXPERIMENTAL SECTION

$Sr_4Fe_3MoO_{12}$ was prepared by the sol−gel method. Stoichiometric amounts of analytical grade $SrCO_3$, $FeC_2O_4{\cdot}2H_2O$, and $(NH_4)_6Mo_7O_{24}.4H_2O$ were dissolved in an aqueous solution of 10% citric acid (10 g of citric acid in 100 mL of water) and 10 mL of nitric acid. The citrate and nitrate solution was slowly evaporated, leading to an organic resin containing a homogeneous distribution of the involved cations. The resin was dried at 120 °C and then decomposed at 600 °C overnight. The organic materials and nitrates were eliminated in a subsequent treatment at 800 °C in the air. This treatment gave rise to a homogeneous precursor material. Then, the precursor was heated in air, in two different steps with intermediate grinding: first at 950 °C for 12 h and finally at 1250 °C for another 12 h. The heating rate was 2 °C/min, and the cooling was inside the furnace after it was shut off. The product was initially characterized by a laboratory powder X-ray diffractometer (PXD; Bruker D8, Cu Kα, λ = 1.5406 Å) for phase identification and to evaluate the phase purity. For the crystal and magnetic structure refinements, we have collected powder neutron diffraction (PND) data at RT and 14 K at the POWGEN instrument[17] in the Spallation Neutron Source at Oak Ridge National Laboratory, Tennessee. The diffraction patterns were analyzed by the Rietveld method, with the Fullprof refinement program.[18,19] In the final run, the following parameters were refined: scale factor, background coefficients, unit-cell parameters, positional coordinates, isotropic thermal parameters, occupancies, and magnitudes of the magnetic moments. The space group determination was supported by electron diffraction with a Phillips CM20 transmission electron microscope, for which the powder was ground, dispersed in ethanol, and deposited on a holey carbon grid. The DC magnetic susceptibility was measured with a commercial SQUID magnetometer on a powder sample, in the temperature range of 1.5−800 K and fields up to 5 T. X-ray absorption near edge spectroscopy (XANES) was collected simultaneously in both the transmission and fluorescence modes on powder samples on beamline X-19A at the Brookhaven National Synchrotron Light Source. Mössbauer studies were performed with a ^{57}Co:Rh source (50 mCi) and a conventional constant acceleration Mössbauer drive in transmission geometry. The absorber was placed either in a cryostat (85 K) or high temperature oven, in a boron nitride holder.

RESULTS

Crystal Structure. We have successfully obtained $Sr_4Fe_3MoO_{12}$ as a black, well-crystallized polycrystalline sample. A single-phase perovskite was identified using PXD (Figure 1). No superstructure peaks corresponding to long-range Fe and Mo ordering were observed; thus the formula can be written as $SrFe_{0.75}Mo_{0.25}O_3$. The structure of $SrFe_{0.75}Mo_{0.25}O_3$ was first reported in a cubic space group $Pm\bar{3}m$,[20] and later it was defined by PND in orthorhombic *Pnma*.[15] However, in the later report, possible tetragonal space groups were rejected, because the refinement of the structure by PND did not converge. We reexamined the structure using PND and electron diffraction and found a different crystal structure, although both compounds, ours and the one previously reported, appear to have nearly identical stoichiometries.

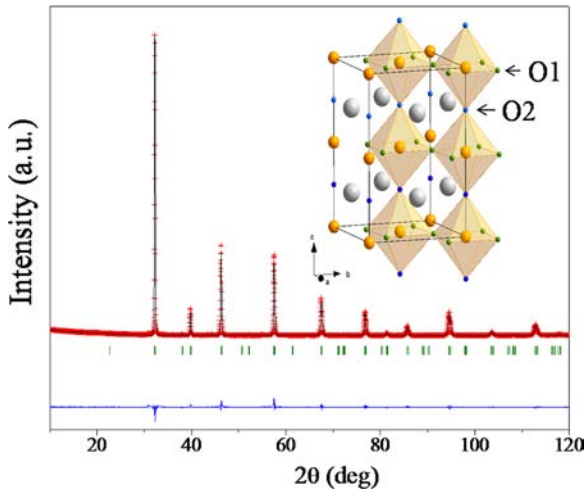

Figure 1. XRD patterns of $SrFe_{0.75}Mo_{0.25}O_{3-\delta}$. The upper inset shows a schematic view of the crystal structure with the gray and bigger spheres corresponding to Sr cations, orange and medium spheres to Fe/Mo, and green and blue smaller spheres to O1 and O2, respectively.

In the high-resolution PND data, the splitting observed in some reflections observed can be explained only by the lowering of the symmetry from cubic to tetragonal (Figure 2).

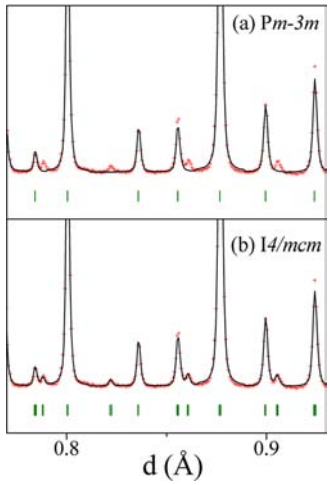

Figure 2. Observed (crosses) and calculated (full line) PND Rietveld profiles at RT of $SrFe_{0.75}Mo_{0.25}O_{3-\delta}$ (a) refined in $Pm\bar{3}m$ and (b) in *I4/mcm*.

The crystal structure was then refined in the tetragonal *I4/mcm* space group (No. 140). The perovskites with this space group belong to a subgroup of the aristotype perovskite with a space group $Pm\bar{3}m$ and may be obtained via an out-of-phase octahedral tilting of BO_6 octahedra along the [001] direction.[21] Using the Glazer notation, it can be described as $a^0a^0c^-$.[22] No other splitting of the diffraction peaks was observed to indicate additional lowering of the symmetry to an orthorhombic space group, and electron diffraction was used to confirm the tetragonal symmetry. The electron diffraction in Figure 3 shows the existence of $\langle 110\rangle_p$ zones (p stands for indexation in the perovskite parent cell) with and without extra reflections at 1/2(ooo) (where o indicates odd indices), while the $\langle 111\rangle_p$ and $\langle 100\rangle_p$ zones all looked the same and showed no extra reflections compared to the $Pm\bar{3}m$ perovskite parent. The 1/

dx.doi.org/10.1021/ic301550m | Inorg. Chem. 2012, 51, 12273−12280

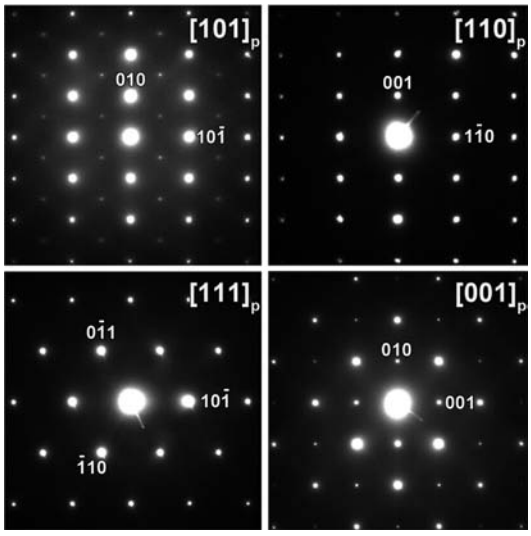

Figure 3. (a) Electron diffraction patterns of $SrFe_{0.75}Mo_{0.25}O_{3-\delta}$ indexed in the parent perovskite cell.

2(ooo) reflections signify the occurrence of antiphase tilts, while the absence of extra reflections in the other zones signifies the absence of in-phase tilts. Together with the occurrence of $\langle 110\rangle_p$ zones with and without extra reflections, this allows one to narrow down the possible tilt systems (with the procedure proposed by Woodward and Reaney:[23] $a^0a^0c^-$, $a^0b^-b^-$, $a^-a^-a^-$, and $a^-b^-b^-$ only, with $a^0a^0c^-$ being the only tetragonal one among these). Therefore, electron diffraction includes the tilt system proposed from PND as one of the four remaining possibilities. Note that the recently published space group *Pnma* ($a^+b^-b^-$)[15] for this compound would result in extra reflections in the $\langle 100\rangle_p$ and $\langle 111\rangle_p$ patterns (at 1/2(eoo) due to the in-phase tilt, and at 1/2(oee) due to the combined presence of in-phase and antiphase tilts (e means even indices)), which were not observed in any of the experimental patterns in our case. We conclude that we have a tetragonal perovskite with the *I*4/*mcm* space group. There are other related perovskites with this space group, e.g., $Sr(Mn_{1/2}Ru_{1/2})O_3$[24] and $Sr(Fe_{1/2}Nb_{1/2})O_3$.[25] This model corresponds to a simple perovskite with only one B site for Fe and Mo cations and two kinds of nonequivalent oxygen atoms (O1 and O2). The O1 and O2 oxygen anions are located in the *ab* plane and along the *c* axis, respectively. The refinement of the possible oxygen deficiency of the sample led to a compound of formula $SrFe_{0.75}Mo_{0.25}O_{2.96(2)}$ with some oxygen vacancies. The oxygen deficiency has been found only in the O1 position, and O2 is stoichiometric as previously reported.[15] The structural parameters, oxygen occupancies, main interatomic distances, and angles at RT and 14 K are listed in Tables 1 and 2. The refinements at 300 and 14 K are in good agreement with the calculated patterns (Figure 4, the second set of reflections shown at 14 K corresponds to the magnetic structure that will be explained below). The schematic structure of $SrFe_{0.75}Mo_{0.25}O_{3-\delta}$ is shown in the upper inset of Figure 1. As we described earlier, the tetragonal structure occurs due to a tilting of the BO_6 octahedra along the *c* direction.

The bond distances obtained from the refinement of the structure are close to those calculated, assuming the effective ionic radii of Shannon:[26] $r_{VI}(Fe^{3+}) = 0.645$ Å, $r_{VI}(Fe^{4+}) = 0.585$ Å, and $r_{VI}(Mo^{6+}) = 0.59$ Å and $r(O^{2-}) = 1.40$ Å and taking into account the formula obtained from PND and the oxidation states from XAS (see below); then the compound is $Sr(Fe_{0.58}{}^{3+}Fe_{0.17}{}^{4+}Mo_{0.25}{}^{6+})_BO_{2.96}$, with the calculated B–O distance of 2.02 Å. We compare the experimentally obtained bond distances with those of similar compounds, such as Sr_2FeMoO_6 or $Sr_3Fe_2MoO_9$: the evolution of the bond distances from Sr_2FeMoO_6 to $Sr_3Fe_2MoO_9$ and finally to $Sr_4Fe_3MoO_{12-4\delta}$ ($SrFe_{0.75}Mo_{0.25}O_{3-\delta}$) is consistent with the decrease of Mo^{6+} content and the increase of the formal oxidation state of Fe ions: in Sr_2FeMoO_6, $\langle Fe^{2+/3+}–O–Mo^{6+/5+}–O/2\rangle$ = 1.974 Å[27] and in $Sr_3Fe_2MoO_9$, $\langle Fe^{3+}–O–$

Table 1. Positional, Thermal Parameters, and Agreement Factors for $SrFe_{0.75}Mo_{0.25}O_{3-\delta}$ after the Rietveld Refinement of NPD Data Collected at 300 and 14 K

	300 K	14 K
*I*4/*mcm*		
a/Å	5.54301(15)	5.53195(16)
b/Å	5.54301(15)	5.53195(16)
c/Å	7.8471(4)	7.8305(4)
V/Å^3	241.103(16)	239.634(16)
Sr		
B/Å^2	0.98(4)	0.62(3)
Fe/Mo		
B/Å^2	0.65(3)	0.52(2)
mag. mom./μ_B		0.85(7)
O1		
x	0.2371(6)	0.2305(3)
y	0.7371(6)	0.7305(3)
B/Å^2	1.2(1)	0.81(3)
occupancy	0.989(7)	0.989(7)
O2		
B/Å^2	1.1(2)	1.0(1)
occupancy	1.00	1.00
reliability factors		
pattern #1		
χ^2	6.19	3.29
R_p (%)	3.79	5.47
R_{wp} (%)	3.69	5.65
R_I (%)	1.48	0.99
$R_{mag.}$ (%)		4.67
pattern #2		
χ^2	3.77	7.37
R_p (%)	6.18	5.15
R_{wp} (%)	6.42	6.24
R_I (%)	3.31	2.30
$R_{mag.}$ (%)		5.27

Table 2. Main Interatomic Distances (Å) and Angles (deg) for $SrFe_{0.75}Mo_{0.25}O_{3-\delta}$ at 300 and 14 K

	300 K	14 K
SrO_8		
Sr–O_1 (×4)	2.702(2)	2.6616(15)
Sr–O_1 (×4)	2.845(2)	2.8771(16)
Sr–O_2 (×4)	2.77150(8)	2.6504(15)
⟨Sr–O⟩	2.7368(1)	2.76597(8)
$(Fe/Mo)O_6$		
(Fe/Mo)–O_1 (×4)	1.962(3)	1.962(2)
(Fe/Mo)–O_2 (×2)	1.96178(10)	1.95763(10)
⟨(Fe/Mo)–O⟩	1.9619	1.9605
angles around O		
(Fe/Mo)–O1–(Fe/Mo)	174.09(14)	171.08(9)
(Fe/Mo)–O2–(Fe/Mo)	180.0	180.0

dx.doi.org/10.1021/ic301550m | *Inorg. Chem.* 2012, 51, 12273–12280

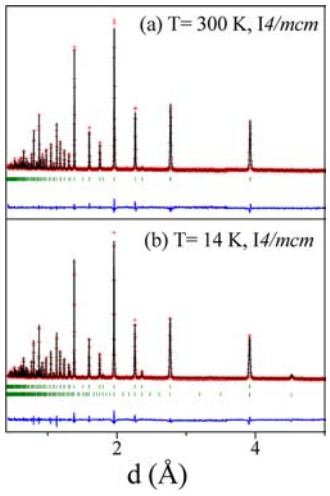

Figure 4. Comparison of the observed (crosses), calculated (solid line), and difference (at the bottom) PND patterns of $SrFe_{0.75}Mo_{0.25}O_{3-\delta}$ at 300 and 14 K. At 14 K, the second set of reflection patterns corresponds to the magnetic structure.

$Mo^{6+}-O/2\rangle$ = 1.97 Å.[28] Therefore, the observed average bond distance $\langle Fe/Mo-O\rangle$ = 1.962 Å in $SrFe_{0.75}Mo_{0.25}O_{3-\delta}$ is consistent with the presence of some Fe^{4+} cations and the consequent reduction of B−O distances. Even if the sample has some oxygen vacancies (as the PND results suggests, i.e., $SrFe_{0.75}Mo_{0.25}O_{2.96}$), the oxidation state of Fe is somewhat greater than 3+ (∼ 3.23+), while that of $Sr_3Fe_2MoO_9$ is formally 3+ (assuming Mo^{6+}), and even smaller in Sr_2FeMoO_6. The bond distance of $SrFeO_3$ (Fe−O = 1.925 Å) is much smaller than in any of the above compounds, because of the higher Fe^{4+} content.[29]

The unit cell parameters of $SrFe_{0.75}Mo_{0.25}O_{3-\delta}$ can also be compared with those of Sr_2FeMoO_6 and $Sr_3Fe_2MoO_9$: for Sr_2FeMoO_6 with the $I4/m$ tetragonal space group, a = 5.56863(5) Å, c = 7.9007(1) Å, and V = 244.999(4) Å^3; for $Sr_3Fe_2MoO_9$ with the same space group, $I4/m$ with Fe and Fe/Mo ordered over the B sites, a = 5.5608(2), c = 7.8471(4) Å, and V = 242.65(2) Å^3; and for $SrFe_{0.75}Mo_{0.25}O_{3-\delta}$ ($Sr_4Fe_3MoO_{12}$), a = 5.54301(15) Å, c = 7.8471(4) Å, and V = 241.103(16) Å^3. Also, the parameters obtained using PND are in good agreement with the parameters obtained using PXD of a = 5.54905(7) Å and c = 7.8444(2) Å. The cell parameters decrease as the content of Mo decreases due to the increase of the formal oxidation state of the Fe ions.

It is also important to comment the obtained oxygen vacancies in the material. The tendency of this compound to oxygen vacancies, which gives its facile bulk oxygen ion diffusivity, has been previously reported.[15] It also has been observed before that the vacancies localize over O1 (oxygen in the *ab* plane) and not over O2 (oxygen over the *c* axis), which are fully occupied. In Table 2, the $(Fe/Mo)-O_1$ bonds are longer than the $(Fe/Mo)-O_2$ ones, thus the oxygen vacancies are localized over the longest B−O distance—an expected result. This could be related to a preferential localization of Fe ions relative to Mo ions around O1 oxygens, since the Fe−O bonds are longer than Mo−O ones and the preferential localization of the vacancies over this position could be well understood in terms of charge differences, since Fe−O bonds are easier to break than Mo−O bonds. This observation has been reported in this compound and in similar ones such as Sr_2FeMoO_6.[15,30] Also it is important to note that O1 is in the position (x y 0) with the possibility of mobility along x and y, while O2 has a fixed position (0 0 1/4); thus the structural positions of the oxygens are also consistent with the easier removal of O1 compared to O2.

XANES. XANES was used to further characterize the formal oxidation state of Fe and Mo in $SrFe_{0.75}Mo_{0.25}O_{3-\delta}$. The $L_{2,3}$ edges of the transition metals (T) manifest intense "white line" (WL) features due to dipole allowed transitions into unoccupied final d states. Specifically, the L_2 and L_3 WL features respectively involve $2p_{1/2} \rightarrow d_{3/2}$ and $2p_{3/2} \rightarrow d_{3/2}/d_{5/2}$ transitions.[31] For 4d and 5d row transition metal compounds, the projected d-symmetry density of states features (weighted by matrix element and the multiplet effects) can be seen in the $L_{2,3}$ spectra.[32−34] The octahedral crystal electric field, CEF (or ligand field), splits the d states in perovskite related compounds into a lower energy 6X degenerate, t_{2g}, and a higher energy 4X degenerate, e_g, state. This CEF splitting is reflected in the splitting of the $T-L_{2,3}$ WL into A (t_{2g}-related) and B (e_g-related) features.

The CEF splitting is particularly large for the perovskites with large B/B′-site valence disparities.[33,34] The $Mo-L_{2,3}$ edges for $SrFe_{0.75}Mo_{0.25}O_3$ (Figure 5) manifest a particularly large

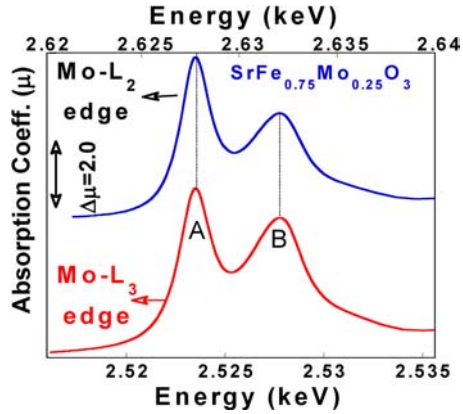

Figure 5. Mo−L_3 and Mo−L_2 edges of $SrFe_{0.75}Mo_{0.25}O_{3-\delta}$. Note the prominent A ($t_{2g}$ related) and B (e_g related) features separated by a ∼4.3 eV CEF splitting.

(∼4.3 eV), well resolved CEF split A−B spectral structure. Relative to 4d and 5d row $L_{2,3}$ XAS, the smaller d-bandwidth and core hole line broadening, along with the better beamline energy resolution at lower energy, all make the Mo A−B spectral structure in Figure 5 particularly sharp. It should be noted that matrix element and multiplet effects make the A feature more prominent in the L_2 edge relative to the L_3 edge.[32] Both the A−B feature structure and the chemical shift of the $T-L_{2,3}$ edge spectra provide information to estimate the T-valence/configuration. Since the L_3 edge is more intense, it will be used for between-compound comparisons for valence/configuration state interrogation.

Figure 6 illustrates the evolution of the $Mo-L_3$ edge structure and chemical shift for a series of octahedral Mo−oxide compounds and elemental Mo. In the sequence of Mo standards, one can see a consistent upward chemical shift with increasing Mo valence and decreasing d count (e.g., see the ∼$4d^0$-Mo^{6+}, MoO_3; ∼$4d^1$-Mo^{5+}, $SrMo_{0.5}Fe_{0.5}O_3$; ∼$4d^2$-Mo^{4+} $Sm_2Mo_2O_7$, and Mo^{0+}, elemental-Mo sequence). In the octahedrally coordinated Mo−O spectra, the chemical shift is indicated by the centers of mass (in energy) of the WL features.

dx.doi.org/10.1021/ic301550m | *Inorg. Chem.* 2012, 51, 12273−12280

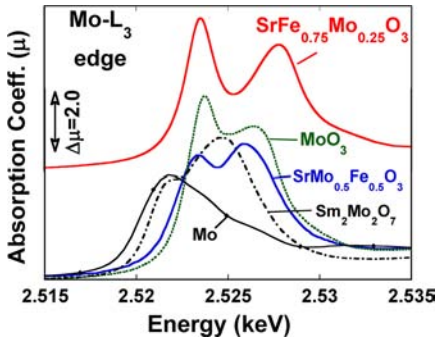

Figure 6. A comparison of the Mo−L_3 edges of $SrFe_{0.75}Mo_{0.25}O_{3-\delta}$ with octahedral standards: ~$4d^0$-Mo^{6+}, MoO_3; ~$4d^1$-Mo^{5+}, $SrMo_{0.5}Fe_{0.5}O_3$; ~$4d^2$-Mo^{4+} Sm_2 Mo_2O_7; along with elemental Mo.

Despite the large CEF splitting, the $SrFe_{0.75}Mo_{0.25}O_{3-\delta}$ can be seen to have a large positive chemical shift, comparable to ~$4d^0$-Mo^{6+} standard MoO_3. Thus the ~$4d^0$-Mo^{6+} state identification is supported by its relative Mo−L_3 edge chemical shift.

The spectral shape electronic configuration indicator, the Mo−L_3 spectra of the perovskite-related compounds (e.g., ~$4d^0$-Mo^{6+}, MoO_3; ~$4d^1$-Mo^{5+}, $SrFe_{0.75}Mo_{0.25}O_{3-\delta}$; and ~$4d^2$-$Mo^{4+}$ $Sm_2Mo_2O_7$) will now be considered. The relative A/B-feature intensities scale with the relative t_{2g}/e_g final d-state hole counts. Indeed, comparison of the spectra shows a clear decrease of relative A-feature intensity with decreasing 4d hole count (increasing 4d electron count) in the ~$4d^0$, ~$4d^1$, ~$4d^2$, and ~$4d^3$ sequence of standard spectra.[34−37] The very intense A-feature intensity in the $SrFe_{0.75}Mo_{0.25}O_{3-\delta}$ spectrum clearly supports a ~$4d^0$-Mo^{6+} state. Thus, the spectral shape again supports Mo^{6+} valence in our compound.

With respect to the K-edge of Fe, both the spectral shape and chemical shift of the main/pre-edge K-edge features can be used as valence state indicators. The main edge peak features are related to dipole transitions into final p states. The pre-edge features are related to transitions into final 3d states via quadruple and p−d hybridization dipole matrix elements. The final state attractive 3d-electron/core-hole interaction shifts these transitions down in energy into the pre-edge region. Figure 7a shows the Fe−K main edge spectra for $LiFePO_4$ (Fe^{2+}), La_2VFeO_6 (Fe^{3+}), and $SrFeO_{3-\delta}$ (~Fe^{4+}) standards (all have corner sharing Fe−O octahedra albeit distorted in the $LiFePO_4$ case).[38,39] The chemical shift of the main edge peak, to higher energy, with increasing valence is clear from the standard spectra. The main edge peak intensity degrades substantially between ~Fe^{3+} and ~Fe^{4+} standards with a more modest chemical shift. Indeed, the loss of intensity and the main edge peak constitute a better indicator of increasing Fe valence in this range than does the chemical shift. This peak degradation is presumably due to strong configuration mixing/covalency causing broadened, split 4p feature in ~Fe^{4+} materials.[40]

The Fe−K pre-edges are shown in Figure 7b with the higher Fe valence compound spectra being displaced downward for clarity. The pre-edges of the sequence Fe^{2+}, Fe^{3+}, and ~Fe^{4+} manifest, with increasing valence: an overall shift in spectral weight toward higher energy, an increase (in most cases) in spectral intensity, and a change in spectral shape. It should be noted that the integrated spectral weight of the $LiFePO_4$ appears relatively enhanced because of the prominent a1 feature. The noncentrosymmetric distortion of the FeO_6 octahedra in this compound could introduce p/d mixing and enhance dipole transitions to the pre-edge features.[39,40] In general, there are two relatively weak and relatively resolved a1−a2 and b1−b2 features in the Fe^{2+} and Fe^{3+} spectra, respectively. The ~Fe^{4+} standard pre-edge manifests three, poorly resolved c1−c2−c3 features. The pre-edge structure spectra of $SrFe_{0.75}Mo_{0.25}O_3$ have a centrum of energy between that of Fe^{3+} and ~Fe^{4+} standard pre-edge spectra. It also shows evidence for a c1−c2−c3 structure as seen in the ~Fe^{4+} standard spectrum. Finally, the intensity of the c1 feature occurs at lower energy and with a greater intensity than that of the ~Fe^{4+} standard. Thus, the pre-edge results are consistent with the Fe−K main edge results and supporting a mixed Fe^{3+}/Fe^{4+} state in the Mo compound. Taken with the ~$4d^0$-Mo^{6+} main edge results, the Fe−K edge results are consistent with the formally $Fe^{3.23+}$ state expected on the basis of the obtained formula $SrFe_{0.75}Mo_{0.25}O_{2.96(2)}$.

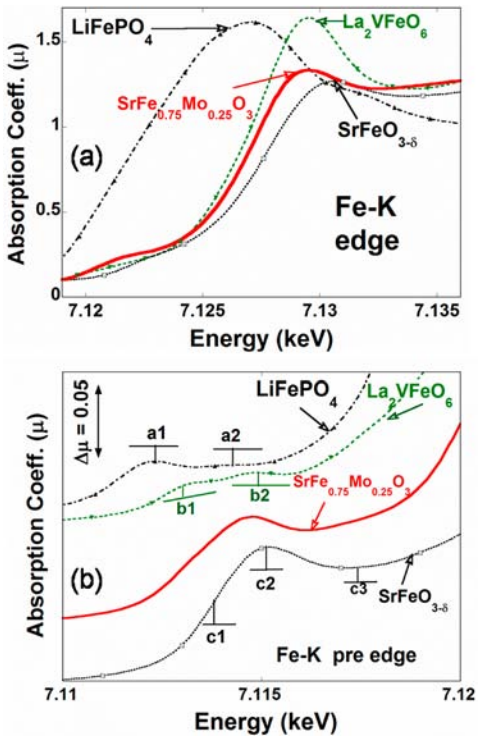

Figure 7. (a) Fe−K main edges of $SrFe_{0.75}Mo_{0.25}O_{3-\delta}$ along with several corner shared octahedral Fe-standard spectra: Fe^{2+}, $LiFePO_4$; Fe^{3+}, La_2VFeO_6; and ~Fe^{4+}, $SrFeO_{3-\delta}$. (b) Fe−K pre-edges for the same compounds.

Magnetic Measurements. The DC susceptibility vs temperature data of $SrFe_{0.75}Mo_{0.25}O_{3-\delta}$ are displayed in Figure 8a. At low temperatures, below 80 K, the zero field cooling (ZFC) and the field cooling (FC) curves diverge, indicating frustration in the system. This frustration could be well understood if we take into account the different magnetic interactions in the material, as will be discussed later. The magnetic susceptibility decreases slowly with increasing temperature until a large change in the slope is observed around 750 K, which indicates the magnetic ordering temperature. This very high ordering magnetic temperature has been previously observed in several comparable complex perovskites, $Sr_3M_2M'O_9$: e.g., $Sr_3Fe_2TeO_9$ (T_N = 717 K) or $Ba_3Fe_2TeO_9$ (T_N = 711 K)[12] and in other very closely related oxides such as the brownmillerite $SrFeO_{2.5}$ (T_N ~ 700 K)[28] or

dx.doi.org/10.1021/ic301550m | Inorg. Chem. 2012, 51, 12273−12280

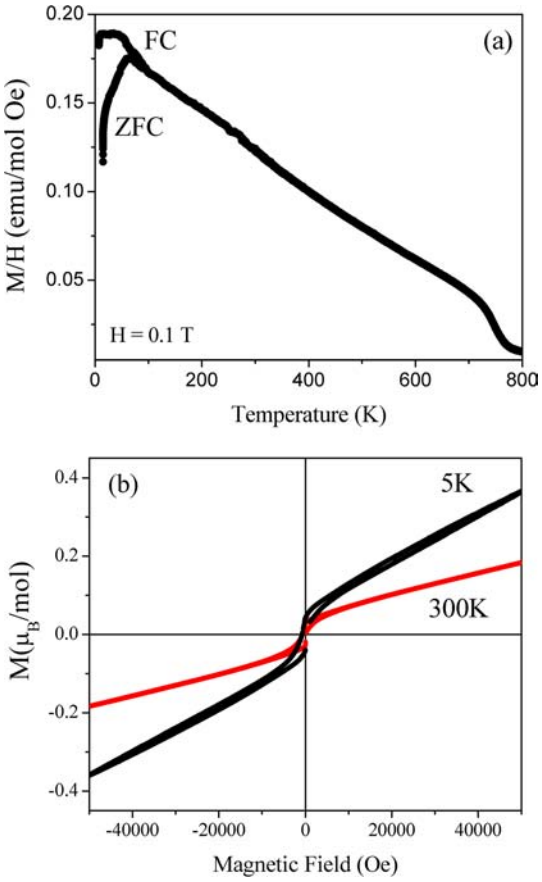

Figure 8. (a) Thermal evolution of the field cooling (FC) and zero field cooling (ZFC) DC susceptibility of $SrFe_{0.75}Mo_{0.25}O_{3-\delta}$. (b) Magnetization vs magnetic field isotherms at 5 and 300 K.

the lanthanum ferrite $LaFeO_3$ ($T_N \sim 750$ K).[41] Since the main magnetic interactions in $SrFe_{0.75}Mo_{0.25}O_{3-\delta}$ are between Fe^{3+} cations, a similar T_N to those found in $SrFeO_{2.5}$ and $LaFeO_3$ is expected.

The onset of magnetic ordering at a high temperature (~750 K) might be ascribed to the presence of Fe-containing impurities, even if no Fe-containing impurities were detected by PXD or PND. However, the magnetic ordering temperatures of all the possible iron oxide impurities are different from what was observed; e.g., Fe_3O_4 (magnetite) is the most probable impurity since the sample was prepared in the air, but it exhibits a very distinct T_C of 850 K.[42] α-Fe_2O_3 (hematite) is a canted antiferromagnet with an even higher T_N of 950 K.[43] β-Fe_2O_3 (maghemite) has a T_C of 920 K and converts to hematite when heated in the air above 750 K. Other possible impurities include $SrFeO_3$ (T_N = 134 K), Sr_2FeMoO_6 ($T_C \sim 420$ K; which has to be prepared in a reducing condition), or $Sr_3Fe_2MoO_9$ (T_C = 330 K).[44,45,26,27] Therefore, we conclude that the observed magnetism is intrinsic to the $SrFe_{0.75}Mo_{0.25}O_{3-\delta}$ perovskite phase, as also will be confirmed by Mössbauer spectroscopy.

The isothermal magnetization curves at 5 K and RT in Figure 8b both exhibit an almost antiferromagnetic response with a small hysteresis characteristic of a weak ferromagnetic component. This ferromagnetic component could be attributed to some canting of the spins or some local ferromagnetic interactions in the compound, since several different magnetic interactions are present between Fe^{3+} and Fe^{4+} cations. For example, some residual ferrimagnetic interactions could occur between Fe^{3+}–O–Fe^{4+}. The magnetic moment obtained from the magnetization curve at 5 K is 0.4 μ_B/mol, which is consistent with the existence of some ferro- or ferrimagnetic interactions in the system.

Magnetic Structure. The establishment of a magnetic ordered phase was studied by PND data measured at 14 K. The low temperature PND pattern shows a weak magnetic contribution of some of the low-angle reflections, e.g. (011) and (211), which could be ascribed to a long-range magnetic ordering between Fe spins. The magnetic intensities have been refined in a model that considers an AFM coupling of Fe^{3+} spins lying along the [100] direction. In the antiferromagnetic structure, a net magnetic moment of 0.85(7) μ_B (Fe atom) at 14 K is in reasonable agreement with the observed remnant magnetization measured at 5 K, of almost 0.4 μ_B (Fe atom; Figure 8b). The refinement of the magnetic structure is shown in Figure 4b, for the data at 14 K. At RT, the magnetic reflections are not observed, since the value of the magnetic moment is too low to be detected by PND (below 0.2 μ_B). However, the susceptibility curve and the hysteresis loop indicate that the material is still magnetic at RT.

Mössbauer Spectroscopy. The Mössbauer spectra of $SrFe_{0.75}Mo_{0.25}O_{3-\delta}$ measured at 763, 673, 300, and 85 K are shown in Figure 9. The velocity calibration and zero velocity in these figures correspond to those measured with a Fe foil. At 85 K, the material is below the magnetic ordering temperature with a broadened magnetic Zeeman sextet and a paramagnetic component, indicating large partial magnetic ordering of the

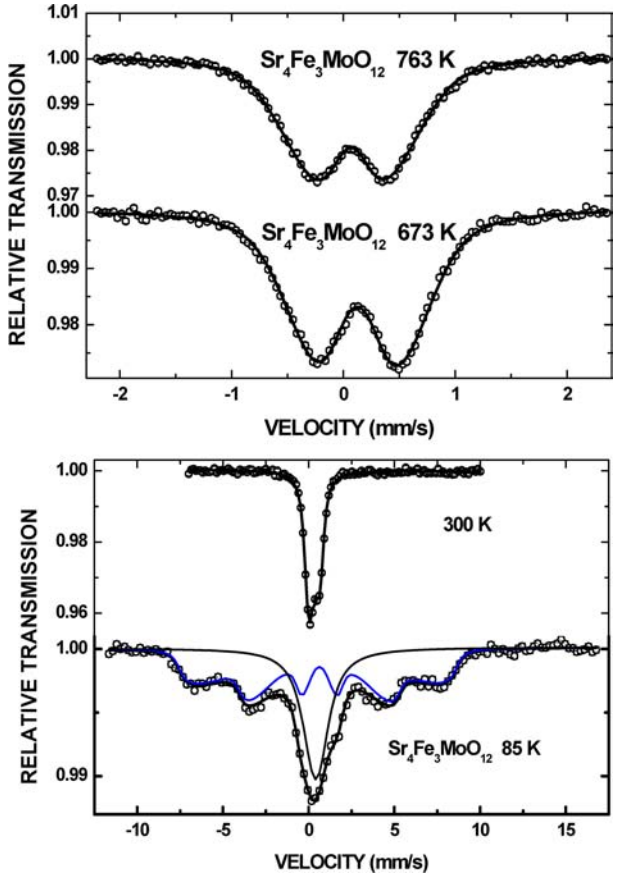

Figure 9. Mössbauer spectrum of $SrFe_{0.75}Mo_{0.25}O_{3-\delta}$ taken at (a) 763 and 673 K and (b) 300 and 85 K.

dx.doi.org/10.1021/ic301550m | Inorg. Chem. 2012, 51, 12273–12280

sample. At 300 K, the doublet is asymmetric, which is usually observed due to the presence of some magnetism. The high temperature spectra show a broad pure doublet at 763 K and an asymmetric broad doublet at 673 K, indicating the possibility of the presence of some remnant magnetism at 673 K. Therefore, the Mössbauer results agree with the PND data, as well as the M(T) results, indicating that the sample is at least partially magnetically ordered near RT, with a very weak magnetic moment. The broadened lines, observed both at low and high temperatures, indicate that the iron ions are in a distribution of different local environments, as expected for such a mixed valent Fe compound.

The origin of this magnetism has to be rationalized. XANES shows a very clear edge of Mo^{6+} and Fe valence between +3 and +4. Therefore, the absence of an itinerant Mo electron prevents the magnetic coupling across Fe−O−Mo paths in such a way that the only possible magnetic superexchange mechanism could take place via Fe−O−Fe paths, in areas of the crystal containing neighboring Fe spins, and since only 1/4 of B positions are occupied by Mo, the magnetic interactions between Fe occurs all over the material with high coherence. Figure 10 shows a simplified image of the proposed magnetic ordering in the sample; only one layer of B cations is shown for the sake of simplicity. An antiferromagnetic coupling between Fe^{3+} spins at both B positions would occur since Fe and Mo cations are completely disordered. Some ferrimagnetic interactions between Fe^{3+} and Fe^{4+} also appear, and finally 1/4 are nonmagnetic Mo^{6+} cations. This disordered magnetic configuration would also explain the observed differences found between ZFC and FC curves (Figure 8a). The many different possible interactions in $SrFe_{0.75}Mo_{0.25}O_{2.96}$ between magnetic Fe^{3+}, Fe^{4+}, and through nonmagnetic Mo^{6+} disordered in three dimensions on the B site of the perovskite structure provide many possible magnetic states, creating frustration in the system.

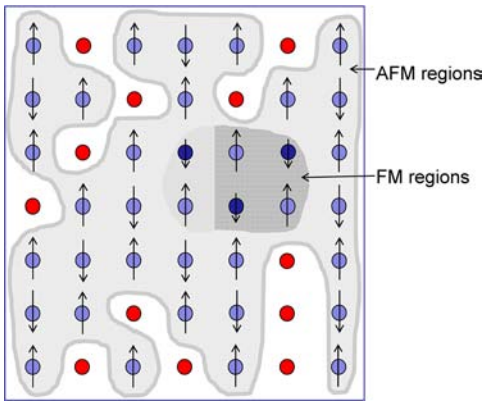

Figure 10. Schematic view of the magnetic interactions in $SrFe_{0.75}Mo_{0.25}O_{3-\delta}$. Fe^{3+} cations are drawn as light blue and with the bigger spins, Fe^{4+} are dark blue and with smaller spins, and the nonmagnetic Mo^{6+} cations are red and without spin.

In contrast to the ordered double perovskites Sr_2FeMoO_6 or $Sr_3Fe_2MoO_9$,[26,27] where there are isolated Fe-rich patches that would lead, on average, to a null saturation magnetization of these areas; in these samples, the Fe−O−Mo−O−Fe areas provide the majority of the magnetization. In our case, the main magnetic interactions are due to the Fe−O−Fe paths, and they are not null. But they are the ones that provide the magnetization to the material and the high T_N. One of the main issues to be addressed in our report is the origin of the magnetic scattering of the sample. The magnetic contributions were fitted to the neutron scattering by modeling an AFM structure consisting of a perfect arrangement of Fe cations occupying all of the B positions of a perovskite structure. The refinement of the magnitude of the magnetic moments on the Fe positions, at 14 K, gives an ordered magnetic moment of 0.85(7) μ_B, with constrained scale factors for the crystal and magnetic structure. Note that this is only the average component of the magnetic moment over all B sites and there are some B sites with nonmagnetic Mo cations that hinder many of the magnetic interactions and decrease strongly the magnetic moment to the value of 0.85(7) μ_B.

■ CONCLUSIONS

The multifunctional perovskite $SrFe_{0.75}Mo_{0.25}O_{3-\delta}$ was characterized in detail. The crystal symmetry was determined to be tetragonal ($I4/mcm$) and not orthorhombic ($Pnma$) as previously reported. $SrFe_{0.75}Mo_{0.25}O_{3-\delta}$ orders antiferromagnetically ($T_N \sim 750$ K), much higher than room temperature. The magnetic structure determined by analysis of the powder neutron diffraction data shows antiferromagnetic coupling between the Fe cations. Mössbauer spectroscopy corroborates the PND results. X-ray absorption spectroscopy indicates the formal oxidation states of the cations to be mixed valent $Fe^{3+/4+}$ and Mo^{6+}.

■ AUTHOR INFORMATION

Corresponding Author

*E-mail: martha@rutchem.rutgers.edu.

Notes

The authors declare no competing financial interest.

■ ACKNOWLEDGMENTS

This work was supported by the NSF-DMR-0966829 grant. We also would like to thank the Spanish Ministry of Education and the Fulbright Commission for the grant of Dr. M. Retuerto. Use of the Spallation Neutron Source is supported by the Division of Scientific User Facilities, Office of Basic Energy Sciences, U.S. Department of Energy, under contract DE-AC05-00OR22725 with UT-Battelle, LLC. Use of the National Synchrotron Light Source, Brookhaven National Laboratory, was supported by the U.S. Department of Energy, Office of Science, Office of Basic Energy Sciences, under Contract No. DE-AC02- 98CH10886.

■ REFERENCES

(1) Steele, B. C. H.; Heinzel, A. *Nature* **2001**, *414*, 345.
(2) Jacobson, A. J. *Chem. Mater.* **2010**, *22*, 660.
(3) Kobayashi, K. I.; Kimura, T.; Sawada, H.; Terakura, K.; Tokura, Y. *Nature* **1998**, *395*, 677.
(4) Ritter, C.; Ibarra, M. R.; Morellón, L.; Blasco, J.; García, J.; de Teresa, J. M. *J. Phys.: Condens. Matter* **2000**, *12*, 8295.
(5) Kim, T. H.; Uehara, M.; Cheong, S.-W.; Lee, S. *Appl. Phys. Lett.* **1999**, *74*, 1737.
(6) Maignan, A.; Raveau, B.; Martin, C.; Hervieu, M. *J. Solid State Chem.* **1999**, *144*, 224.
(7) Borges, R. P.; Thomas, R. M.; Cullinan, C.; Coey, J. M. D.; Suryanarayan, R.; Ben-Dor, L.; Pinsard-Gaudart, L.; Revcolevschi, A. *J. Phys.: Condens. Matter* **1999**, *11*, L445.
(8) Kobayashi, K. I.; Kimura, T.; Tomioka, Y.; Sawada, H.; Terakura, K.; Tokura, Y. *Phys. Rev. B* **1999**, *59*, 11159.
(9) Ritter, C.; Ibarra, M. R.; Morellón, L.; Blasco, J.; García, J.; De Teresa, J. M. *J. Phys: Condens. Matter.* **2000**, *12*, 8295.

(10) Pinacca, R. M.; Viola, M. C.; Alonso, J. A.; Pedregosa, J. C.; Carbonio, R. E. *J. Mat. Chem.* **2005**, *15*, 4648.
(11) Viola, M. C.; Alonso, J. A.; Pedregosa, J. C.; Carbonio, R. E. *Eur. J. Inorg. Chem.* **2005**, 1559.
(12) Ausburger, M. S.; Viola, M. C.; Pedregosa, J. C.; Carbonio, R. E. *J. Mat. Chem.* **2006**, *16*, 4235.
(13) Xiao, G.; Liu, Q.; Zhao, F.; Zhang, L.; Xia, C.; Chen, F. *J. Electrochem. Soc.* **2011**, *158*, B455.
(14) Liu, Q.; Bugaris, D. E.; Xiao, G.; Chmara, M.; Ma, S.; zur Loye, H.-C.; Amiridis, M. D.; Chen, F. *J. Power Sources* **2011**, *196*, 9148.
(15) Munoz-Garcia, A. B.; Bugaris, D. E.; Pavone, M.; Hodges, J. P.; Huq, A.; Chen, F.; zur Loye, H.-C.; Carter, E. A. *J. Am. Chem. Soc.* **2012**, *134*, 6826.
(16) Liu, Q.; Dong, X.; Xiao, G.; Ma, S.; Zhao, F.; Chen, F. *Adv. Mater.* **2010**, *22*, 5478.
(17) Huq, A.; Hodges, J. P.; Gourdon, O.; Heroux, L. *Z. Kristallogr. Proc.* **2011**, *1*, 127.
(18) Rietveld, H. M. *J. Appl. Crystallogr.* **1969**, *2*, 65.
(19) Rodríguez-Carvajal, J. *Physica B* **1993**, *192*, 55.
(20) Markov, A. A.; Leonidov, I. A.; Patrakeev, M. V.; Kozhevnikov, V. L.; Savinskaya, O. A.; Ancharova, U. V.; Nemudry, A. P. *Solid State Ionics* **2008**, *179*, 1050.
(21) Howard, C. J.; Kennedy, B. J.; Woodward, P. M. *Acta Crystallogr.* **2003**, *B59*, 463.
(22) Glazer, A. M. *Acta Crystallogr.* **1972**, *B28*, 3384.
(23) Woodward, D. I.; Reaney, I. M. *Acta Crystallogr.* **2005**, *B61*, 387.
(24) Lufaso, M. W.; Woodward, P. M.; Goldberger, J *J. Solid State Chem.* **2004**, *177*, 1651.
(25) Lufaso, M. W.; Macquart, R. B.; Yong, J. L.; Vogt, T; zur Loye, H. C. *J. Phys.: Condens. Matt.* **2006**, *18*, 8761.
(26) Shannon, R. D. *Acta Crystallogr., Sect. A* **1976**, *32*, 751.
(27) Retuerto, M.; Alonso, J. A.; Martínez-Lope, M. J.; Martínez, J. L.; García-Hernández, M. *Appl. Phys. Lett.* **2004**, *85*, 266.
(28) Viola, M. C.; Alonso, J. A.; Pedregosa, J. C.; Carbonio, R. E. *Eur. J. Inorg. Chem.* **2005**, 1559.
(29) Takeda, Y.; Kanno, K.; Tabada, T.; Yamamoto, O.; Takano, M.; Nakayama, N.; Bando, Y. *J. Sol. St. Chem.* **1986**, *63*, 237.
(30) Muñoz-Garcia, A. B.; Pavone, M.; Carter, E. A. *Chem. Mater.* **2011**, *23*, 4525.
(31) Qi, B.; Perez, I.; Ansari, P. H.; Lu, F.; Croft, M. *Phys. Rev.* **1987**, *B36*, 2972.
(32) Ruckman, M. W.; Reisfeld, G.; Jisrawi, N.; Weinert, M.; Strongin, M.; Weismann, H.; Croft, M.; Sahiner, A.; Sills, D.; Ansari, P. *Phys. Rev.* **1998**, *B57*, 3881.
(33) de Groot, F. M. F. *Physica B* **1995**, *208&209*, 15.
(34) Yang, T.; Perkisas, T.; Hadermann, J.; Croft, M.; Ignatov, A.; Greenblatt, M. *J. Solid State Chem.* **2010**, *183*, 2689.
(35) Veith, G. M.; Greenblatt, M.; Croft, M.; Goodenough, J. B. *Mater. Res. Bull.* **2001**, *36*, 1521−1530.
(36) Ramanujschary, K.; Lofland, S.; McCarroll, W.; Emge, T; Greenblatt, M.; Croft, M. *J. Solid State Chem.* **2002**, *164*, 60.
(37) Veith, G. M.; Lobanov, M. V.; Emge, T. J.; Greenblatt, M.; Croft, M.; Stowasser, F.; Hadermann, J.; Van Tendeloo, G. *J. Mater. Chem.* **2004**, *14*, 1623.
(38) Liang, G.; Park, K.; Li, J.; Benson, R.; Vaknin, D.; Markert, J. T.; Croft, M. *Phys. Rev.* **2008**, *B77*, 064414.
(39) Zhang, L.-L.; Liang, G.; Ignatov, A.; Croft, M.; Xiong, X.-Q.; Hung, I.-M.; Huang, Y.-H.; Hu, X.-L.; Zhang, W.-X.; Peng, Y.-L. *J. Phys. Chem. C* **2011**, *115*, 13520.
(40) Veith, G.; Chen, R.; Popov, M.; Greenblatt, M.; Croft, M.; Nowik, I. *J. Solid State Chem.* **2002**, *166*, 292.
(41) Scholl, A.; Stohr, J.; Luning, J.; Seo, J. W.; Fompeyrine, J.; Siegwart, H.; Locquet, J.-P.; Nolting, F.; Anders, S.; Fullerton, E. E.; Scheinfein, M. R.; Padmore, H. A. *Science* **2000**, *287*, 1014.
(42) Greenwood, N.; Earnshaw, A. *Chemistry of the Elements*; Butterworth-Heinemann: Oxford, U. K., 1997.
(43) Harrison, R. J. *Rev. Mineral.* **2000**, *39*, 175.
(44) Gallagher, P. K.; MacChesney, J. B.; Buchanan, D. N. E. *J. Chem. Phys.* **1964**, *41*, 2429.
(45) MacChesney, J. B.; Sherwood, R. C.; Potter, J. F. *J. Chem. Phys.* **1965**, *43*, 1907.